Surface Science 720 (2022) 122052

Contents lists available at ScienceDirect

Surface Science

journal homepage: www.elsevier.com/locate/susc

Defects investigation of bipolar exfoliated phosphorene nanosheets

Amin Rabiei Baboukani [a], Sadegh Mehdi Aghaei [b], Iman Khakpour [a], Vadym Drozd [a,c], Aref Aasi [b], Chunlei Wang [a,c,*]

[a] Department of Mechanical and Materials Engineering, Florida International University, Miami, FL 33174, USA
[b] Small Systems Laboratory, Department of Mechanical Engineering, Worcester Polytechnic Institute, Worcester, MA 01609, USA
[c] Center for the Study of Matter of Extreme Conditions (CeSMEC), Florida International University, Miami, FL 33199, USA

ARTICLE INFO

Keywords:
Phosphorene
Defect
Transmission electron microscopy
Bipolar electrochemistry
Density functional theory

ABSTRACT

Two-dimensional (2D) phosphorene has gained attention due to its exceptional chemical, physical, and opto-electronic properties. However, defects analysis in exfoliated phosphorene through experimental techniques is still largely missing. In this paper, a combination of high-resolution transmission electron microscopy (HRTEM) imaging and density functional theory calculations were provided to study the point defects, grain boundaries (GBs), and amorphization phenomenon in exfoliated phosphorene nanosheets *via* bipolar electrochemistry method. The HRTEM results demonstrate that the single vacancies (SV) and di-vacancies (DV), ad-atoms, and GBs defects are formed in phosphorene nanosheets. However, the exfoliated black phosphorus nanosheets maintained its orthorhombic crystal structure. In addition, amorphization on the edges and surface of nanosheets is unavoidable in the presence of oxygen. Our first-principles simulation confirms the breakage of P-P bonds of phosphorene upon surface oxidation, which results in amorphization. The defect analysis of phosphorene nanosheets obtained from this study could benefit both fundamental research and technological applications.

1. Introduction

Motivated by the discovery of graphene [1], other diversified atomically thin two-dimensional (2D) materials such as transition metal dichalcogenides (TMDs) [2], hexagonal boron nitride (hBN) [3], and layered transition metal oxides [4] have been evaluated for different applications due to their distinctive properties. Black phosphorus (BP) nanosheet (so-called phosphorene), as a unique member of 2D materials, has recently attracted considerable attention due to its physical and chemical properties [5–7]. In the structure of BP, each P atom is connected to three neighboring P atoms covalently and forms a honeycomb puckered layered structure with an interlayer distance of about 0.53 nm [8]. BP can be exfoliated into a few or monolayer of 2D BP nanosheets through bottom-up and top-down techniques [9,10]. Compared to the expensive and low-yield bottom-up methods, mechanical and liquid-based exfoliations of BP into phosphorene nanosheets have been successfully demonstrated in numerous studies [5, 11]. Very recently, we developed a novel bipolar electrochemical (BPE) approach for simultaneous exfoliation and deposition of phosphorene nanosheets on conductive substrates [12,13].

In general, 2D materials inevitably incorporate different structural defects such as point defects, grain boundaries (GBs), impurities, and dislocations [14–16]. Due to the non-negligible effect of structural defects on the physical, chemical, and optical properties of 2D materials, investigating the defect structure is essential for further practical applications [17]. Besides, through the defect engineering of 2D materials, their properties can also be tailored for specific applications [18]. With the rapid progress in high-resolution transmission electron microscopy (HRTEM) as the most commonly used techniques, 2D materials have extensively been characterized in terms of atomic structure, the motion of atoms, chemical composition, and structure transformations in real-time [19, 20]. Moreover, large area diffraction can be performed to evaluate the crystallinity of exfoliated materials with atomic resolution [21]. Direct evidence by HRTEM analysis has revealed the various types of defects, the modulation of the electronic structure and dopants within the lattice of their monolayer of graphene, TMDs, and hBN [22,23]. Although invariable degradation of phosphorene nanosheets has been reported [24–27], its in-details defect characterization using TEM is still missing.

Recently, Density Functional Theory (DFT) calculations have been employed to evaluate the defects formation and their stability on the phosphorene nanosheets. DFT calculations predict different types of

* Corresponding author.
E-mail address: wangc@fiu.edu (C. Wang).

https://doi.org/10.1016/j.susc.2022.122052
Received 9 August 2021; Received in revised form 9 February 2022; Accepted 10 February 2022
Available online 11 February 2022

defects in phosphorene nanosheets with intriguing electronic properties [28]. For example, Wang and co-workers predicted the various stable defects such as single vacancies (SVs), double vacancies (DVs), and self-interstitials [29]. Theoretical calculations confirmed that the formation energies of these point defects are much lower compared to those in graphene, hBN, and TMDs [30]. On the other hand, Li et al. demonstrated that the migration and aggregation of point defects such as anisotropic SVs and DVs provided GBs between domains of different orientations in phosphorene nanosheets [31]. The formation energy of less than 1.5 eV nm ^{1} reveals the thermodynamically stable phosphorene GBs [32].

In this study, we conducted the TEM investigation for the BPE exfoliated phosphorene nanosheets and obtained direct evidence of point defects, GBs, and amorphous regions on the phosphorene. Moreover, DFT calculations reveal that the amorphization occurs as a result of surface oxidation of phosphorene. Combining TEM analysis and DFT calculation provides new insight to understand the effect of the BPE method on defect formation and surface properties of phosphorene nanosheets.

2. Materials and methods

The schematic and in-details setup for the bipolar exfoliation of BP into phosphorene has been reported in our previous study [12]. In brief, a 1 cm long and 3 mm in diameter bulk BP bar (99.998% purity from Smart-Elements) was placed between the two 316 stainless steel feeding electrodes (1×2 cm^2) in deionized water. The 30 Vdc (i.e., an electric field of 10 V cm ^{1}) was applied between the two feeding electrodes for 24 hours under an ambient environment using a multichannel DC power analyzer (Agilent Technologies N6705A).

After the bipolar exfoliation process, the dispersed phosphorene nanosheets were collected with deionized water for HRTEM analysis (model Tecnai TF 20 TEM). The HRTEM analysis was conducted at an accelerating voltage of 200 kV, using a field emission gun with a 0.2 nm resolution. For the sample preparation, after the separation and dispersion of phosphorene nanosheets through sonication, one droplet of the solution was transferred on the TEM grid covered by formvar carbon transparent film, and next, the TEM grids were stored in a dry atmosphere to remove the remaining liquids.

The first-principles density functional theory (DFT) calculations were performed by Atomistix ToolKit (ATK) package [33–35] using Generalized Gradient Approximation of Perdew–Burke–Ernzerhof (GGA-PBE) functionals with a double-ζ polarized basis set. The van der Waals (vdW) force is not correctly described with the PBE functional. The long-range vdW interaction was included through the semi-empirical corrections by Grimme D2 correction, which is computationally less demanding than D3 correction [36,37]. A supercell of monolayer phosphorene that contains 64 phosphorus atoms was assumed (Fig. S1a). A vacuum space of 2 nm was added on both sides of the phosphorene plane in the direction that the sheet is not periodic (ʒ) in order to avoid the image-image interactions. The oxygen atom was placed on various adsorption sites (top of phosphorus atoms, above hollow site, and top of a bridge between two phosphorus atoms) on phosphorene. All the possible structures were fully relaxed using the limited-memory Broyden-Fletcher-Goldfarb-Shanno (LBFGS) quasi-Newton method [38], with 0.01 eV/Å force tolerance and 0.001 eV/Å^3 stress tolerance. The electronic temperature was 300 K and the density mesh cut-off was set to be 125 Rydberg. Moreover, Monkhorst-Pack k-points mesh [39] of 5 × 5 × 1 and 11×11×1 were used to sample the Brillouin zones during geometry optimization and to calculate the total energy and the electronic band structures. Besides vdW interactions, since our systems have two subsystems: the phosphorene sheet (A) and the oxygen atoms (B), incompleteness of the Linear Combination of Atomic Orbitals (LCAO) basis set can give rise to a so-called basis set superposition error (BSSE). In an isolated A system, only the basis orbitals in the A system describe it. While, A and B are coupled, the basis orbitals in the system B will also be used to describe system A, resulting in a larger available basis set for system A. To remove BSSE, a counterpoise (cp) correction was added to the total energy [40]. The adsorption energy per oxygen atom on the phosphorene sheet was calculated using Eq. (1) to find the most stable adsorption configuration (with the most negative adsorption energy).

$$E_{ad} = \frac{1}{n}\left[E_{Phosphorene+nO} \quad \left(E_{Phosphorene} + n \times \frac{1}{2} \times E_{O_2}\right)\right] \tag{1}$$

where n, $E_{Phosphorene\ +\ nO}$, $E_{Phosphorene}$, and E_{O_2} are the number of O atoms, total energies of the phosphorene-n oxygen atoms complex, pristine phosphorene sheet, and the isolated oxygen molecule, respectively. It should be mentioned that the energy of O_2 molecule was used as a reference state instead of atomic O because the use of oxygen atoms as the reference does not necessarily correspond to the experiments, where there are no free oxygen atoms to react with the surface.

3. Results and discussion

Similar to other 2D materials, phosphorene nanosheets could be damaged by electron irradiation during the TEM investigation. In order to obtain atomic-resolution images from the phosphorene nanosheets, the exposure of the material to the electron beam has to be minimized. The TEM images of the phosphorene nanosheets collected from DI water after 24-hour BPE exfoliation are shown in Fig. 1 (a-c) and Fig. 2 (a-d). The interplanar distances and the corresponding Miller indices are labeled on the TEM images. The exfoliated phosphorene nanosheets revealed different lattice fringes with interplanar distances of 0.21, 0.34, 0.25, and 0.23 nm, which could be assigned to the (002), (021), (111), and (041) atomic planes of orthorhombic BP crystal structure (JCPDS no 96-101-0326) [12]. These various plane orientations and domains of phosphorene nanosheets indicate the polycrystalline nature of the bulk BP. It is clear from the TEM images that the crystal structure of phosphorene nanosheets appears to be not affected much during the BPE exfoliation. However, as shown in Fig. 1 (a), point defects as SVs and DVs are present in phosphorene nanosheets (black patches indicated by red dashed circles). As shown in Fig. 1(a), the smallest defect located at the center of the image and labeled in red as (1) is related to the SV. According to the DFT calculations, the simplest type of defect in phosphorene nanosheets is the missing of one or two lattice atoms [28]. In general, the removal of a single phosphorus atom in a phosphorene nanosheet and creating three dangling atoms distributed in two neighbors can form SVs on the nanosheet. The DVs labeled in red as (2) in Fig. 1(a) could be created either by removing two neighboring phosphorus atoms or by coalescence of two SVs during the exposure of exfoliated phosphorene nanosheets to ambient environment or inside the TEM chamber [30]. Kistanov et al. theoretically demonstrated that the SVs and DVs, which consist of pentagon-nonagon (59) and pentagon-heptagon-pentagon-heptagon (5757) rings, are the most common point defects in phosphorene nanosheets from the viewpoint of energetic stability [41].

Fig. 1 (b) shows a few heavier bright atoms sprinkled over the whole surface of the phosphorene nanosheets, which are impurities as an adatom defect. The zoomed-in TEM image confirmed the presence of adatom. However, its origin is not entirely clear. It might be present due to the contact with sample preparation equipment impurity atoms in the TEM chamber or it could be introduced during the BPE exfoliation process where the stainless steel as a feeding electrode in DI-water were used. Clarification of this issue requires the employment of additional analytical methods, i.e., electron energy loss spectroscopy (EELS) which has been successfully employed to characterize impurities on the atomic scale in other 2D materials [42]. The zoomed-in TEM image in Fig. 1(b) revealed the honeycomb crystal structure of phosphorene nanosheets where each phosphorus atom is distinguished, and the pattern is repeated throughout the image.

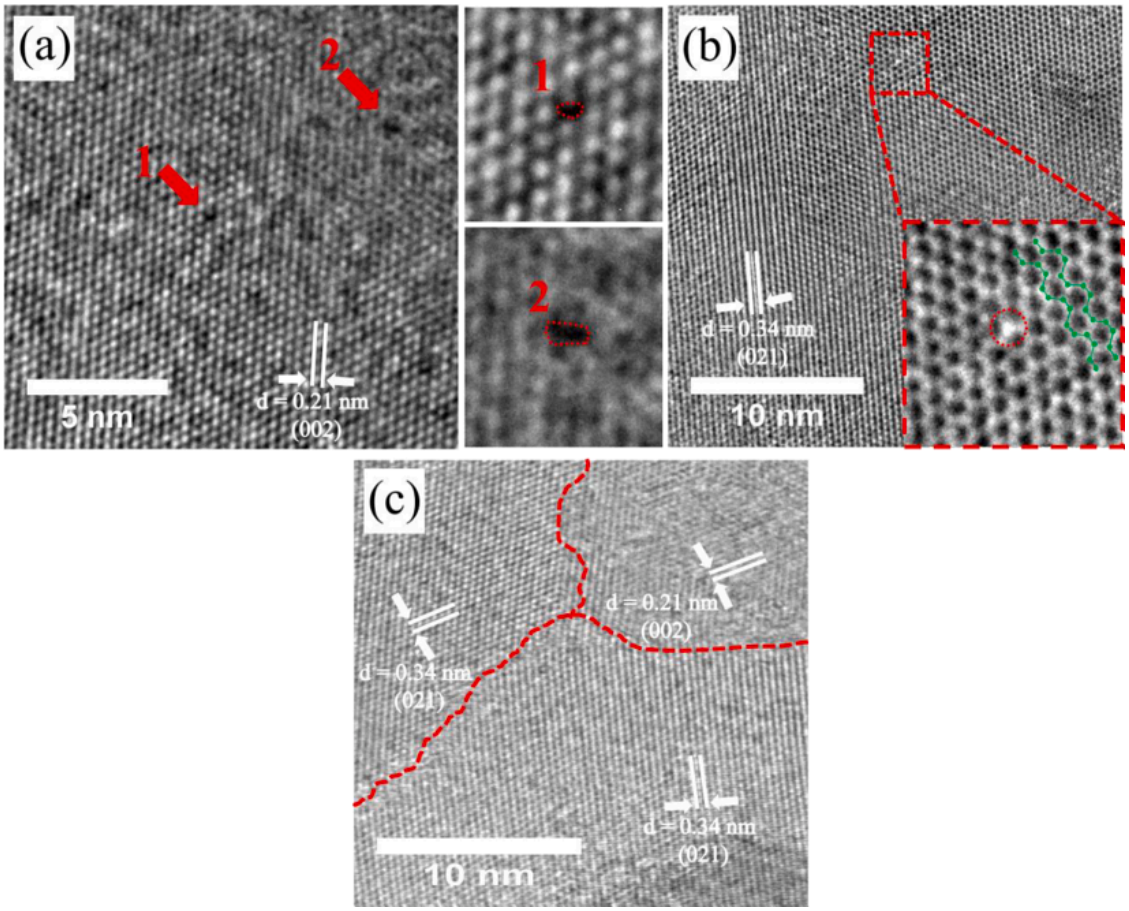

Fig. 1. HRTEM images of (a) intrinsic SV and DV, (b) ad-atom, and (c, d) GB defects in phosphorene nanosheets obtained via bipolar electrochemistry method.

Fig. 1 (c) shows the GBs defect composed of linear dislocation arrays of the (021) and (002) atomic planes of exfoliated phosphorene nanosheets. The main reason for the GB formation in 2D materials is typically related to the polycrystalline nature of bulk material. As shown in Fig. 1 (c), the GB region presents larger brightness than the rest of the nanosheet because of the high partial charge density around the GBs. Liu and co-workers theoretically confirmed that the GB energies in phosphorene nanosheets are lower than those in graphene, TMDs, and hBN [32]. This suggests higher stability of phosphorene nanosheets against lattice distortions compared to other 2D materials. Moreover, in a theoretical study by Zhu et al., high reactivity of GB regions with O atom as an impurity in phosphorene nanosheets has been confirmed. The GB defects in phosphorene do not have a significant effect on its electronic properties [16, 43]. The TEM images of the exfoliated phosphorene nanosheets via BPE method confirmed that the atomic network remains coherent with minor perturbations in the bond lengths.

Fig. 2 (a-d) shows the TEM images of phosphorene nanosheets with amorphous regions, which are most likely produced during the exfoliation of BP in DI water or exposure of nanosheets during sample preparation for TEM. The uniform amorphous layer can be easily visualized on the edge of (021) phosphorene nanosheets with less than 10nm thickness, as shown in Fig. 2 (a, c). In Fig. 2(b), an amorphous domain with a size of about 10nm could be found in another (021) nanosheet. The instability of the phosphorene nanosheets upon exposure to the ambient environment was initially evaluated by theoretical calculations [44]. Several studies have shown that oxygen and water degrade the phosphorene nanosheets [45–47]. Previous studies also confirmed that the phosphorene nanosheet rapidly degraded in vacuum at 300 kV accelerating voltage of e-beam [24]. The TEM images of phosphorene nanosheets obtained via BPE method revealed relatively good stability under the accelerated voltage of 200 kV. Fig. 2 (a, c) shows the oxidation and amorphization on the edges of the phosphorene nanosheet, which is likely related to the presence of phosphorus oxide along the edge of the nanosheets. The amorphous domains on the phosphorene nanosheet in Fig. 2 (b) may be related to the polycrystalline nature of bulk BP. However, e-beam could also create oxygen radicals and degrade the phosphorene nanosheets. Especially, the phosphorus atoms on the surface do not have to be squeezed into an interstitial site; as a result, they are free to leave the nanosheets and then enter the chamber of the microscope. The theoretical calculations confirmed that due to the low displacement threshold in phosphorene nanosheets, even an 80 kV beam should rapidly provide considerable damage [48]. Fig. 2 (d) shows the degradation and amorphization of phosphorene nanosheets after 4 days' exposure to air. The TEM image shows that numerous small fringes of BP crystalline structure with an interplanar spacing of 0.23 nm and 0.25 nm corresponding to the (041) and (111) planes, which are embedded in the disordered amorphous structure. Degradation of the sample exposed to ambient atmosphere confirms the high sensitivity of phosphorene nanosheets to oxygen and/or water molecules.

The stability of the pristine phosphorene sheet in the presence of atomic oxygen was investigated by DFT calculations to further comprehend the degradation of the nanosheets during the BPE exfoliation, their storage, and handling process. The lattice constants for a monolayer of phosphorene were found to be $a = 0.332$ nm, $b = 0.441$ nm, and the bandgap was calculated to be ~ 0.92 eV at the Γ point of the Brillouin zone, as shown in Fig. S1 that is in agreement with the GGA-PBE studies [49,50]. However, it should be mentioned that the bandgap is underestimated in GGA calculations [51]. Due to the electron lone pair on the P atoms on the surface of phosphorene, P atoms are preferential sites to form bonds with O atoms. For the adsorption of a

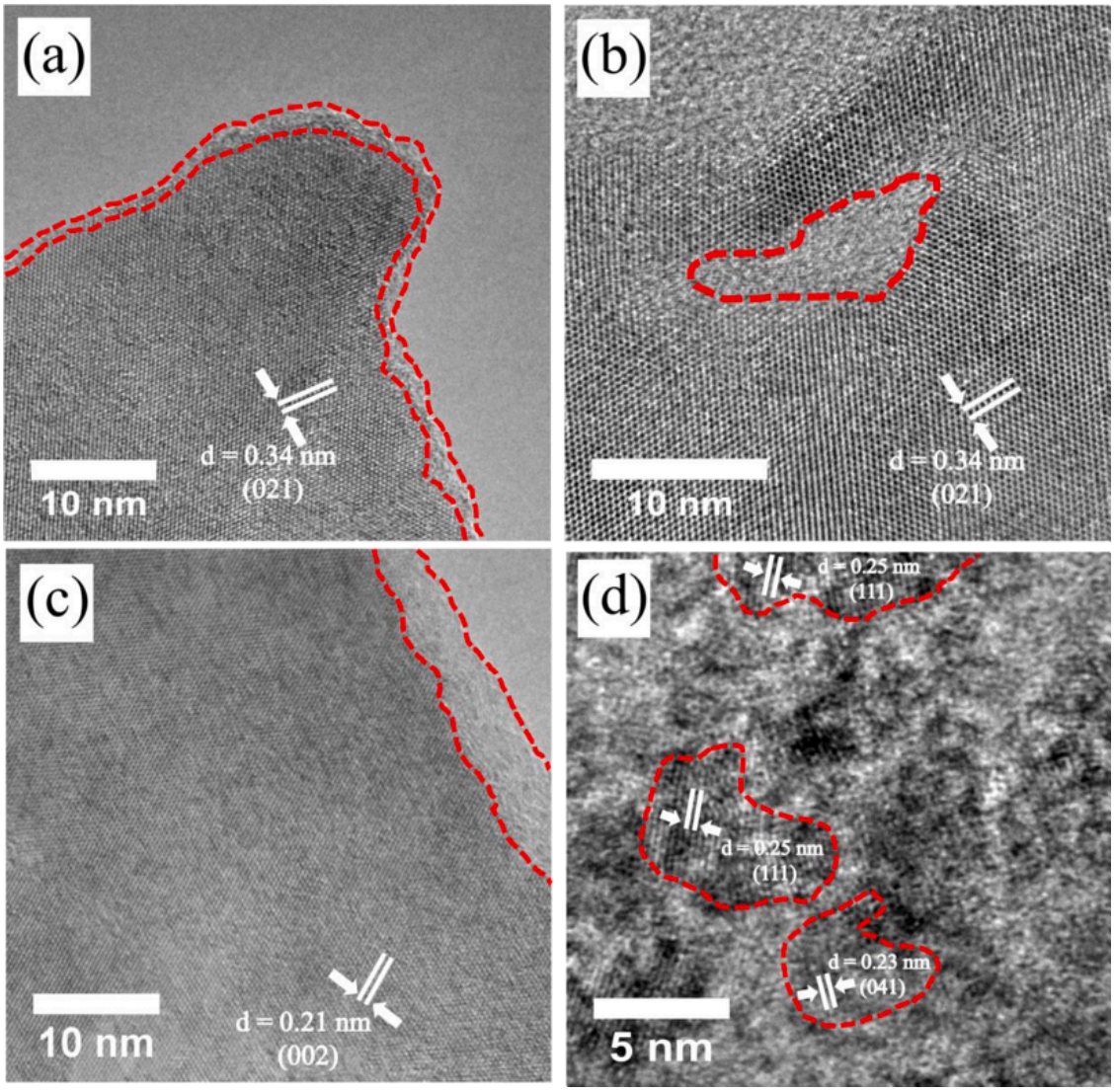

Fig. 2. HRTEM images of (a-c) amorphization on the edges and surfaces, and (d) degradation of phosphorene nanosheets after 4 days of exposure to the ambient environment. The boundary between crystalline and amorphous regions is marked by red dashed lines.

single oxygen atom, the most energetically favorable position was found to be on top of a phosphorus atom in the phosphorene's top sublattice (with P-O bond length of 0.152 nm and O-P-P angle of 113.0°, as shown in Fig. 3 (a)). The large adsorption energy of 2.93 eV suggests that phosphorene can be easily oxidized through an oxygen atom's chemisorption. This agrees with [52] where oxygen atoms are chemisorbed in a dangling configuration with P-O bond length of 0.150 nm and binding energy of 2.08 eV (PBE). The reason for the discrepancy between the obtained adsorption energy and value in the literature includes both Grimme correction and counterpoise correction in our calculations. We previously showed that the absolute values of adsorption energies calculated by PBE+D2+cp are significantly larger than that of PBE approximation [53].

The most stable adsorption configurations for phosphorene oxide sheets with various oxygen concentrations (1-32) are provided in Fig. S2, and their adsorption energies are listed in Table 1. For 2, 4, 8, 12, and 16 oxygen atoms, more than one adsorption configuration was considered (Fig. S3 and Table S1) to maximize the distance between the oxygen atoms on the phosphorene layer. Fig. 3 (b) shows the change in adsorption energy per oxygen atom on the monolayer phosphorene as a function of the oxygen concentration. With increasing the number of oxygen atoms in the supercell, the adsorption energies first increase (the structure becomes less stable) to 2.86 eV (for 4 oxygen atoms), then decrease (the structure becomes more stable) to 2.87 eV (for 8 oxygen atoms), are almost constant (1 meV fluctuations) for 8, 12, and 16 oxygen atoms, where half of phosphorus atoms in the top sublattice of the phosphorene are oxidized. By increasing the number of oxygen atoms from 16 to 32 (where all the phosphorus atoms on the top side were oxidized), the adsorption energy was decreased with the rate of 0.028 eV/oxygen atom and reached 2.41 eV for 32 oxygen atoms. The most stable adsorption configurations for phosphorene oxide sheets with various oxygen concentrations (1-32) were provided in Fig. S2, and their adsorption energies were listed in Table 1. While the phosphorene nanosheet retains its initial puckered structure for 1-28 adsorbed oxygen atoms, its structure was distorted upon adsorption of 32 oxygen atoms, as shown in Fig. 3a. Phosphorene oxidation involving the dissociative chemisorption of O_2 causes the decomposition of phosphorene [46,54]. From Fig. S4, one can see that fraction of oxygen atoms (dangling oxygens) is adsorbed at the top site with P-O bond length of 0.149 nm and O-P-P bond angle of 133.6°, while others (binding oxygens) are embedded in the bridge between two phosphorous atoms with P-O bond lengths of 0.163 nm and 0.170 nm and P-O-P bond angle of 111.4°, resulting in cleavage of P-P bonds. The P-P bond length changed from 0.224 nm in bare phosphorene to 0.287 nm in phosphorene with 32 O

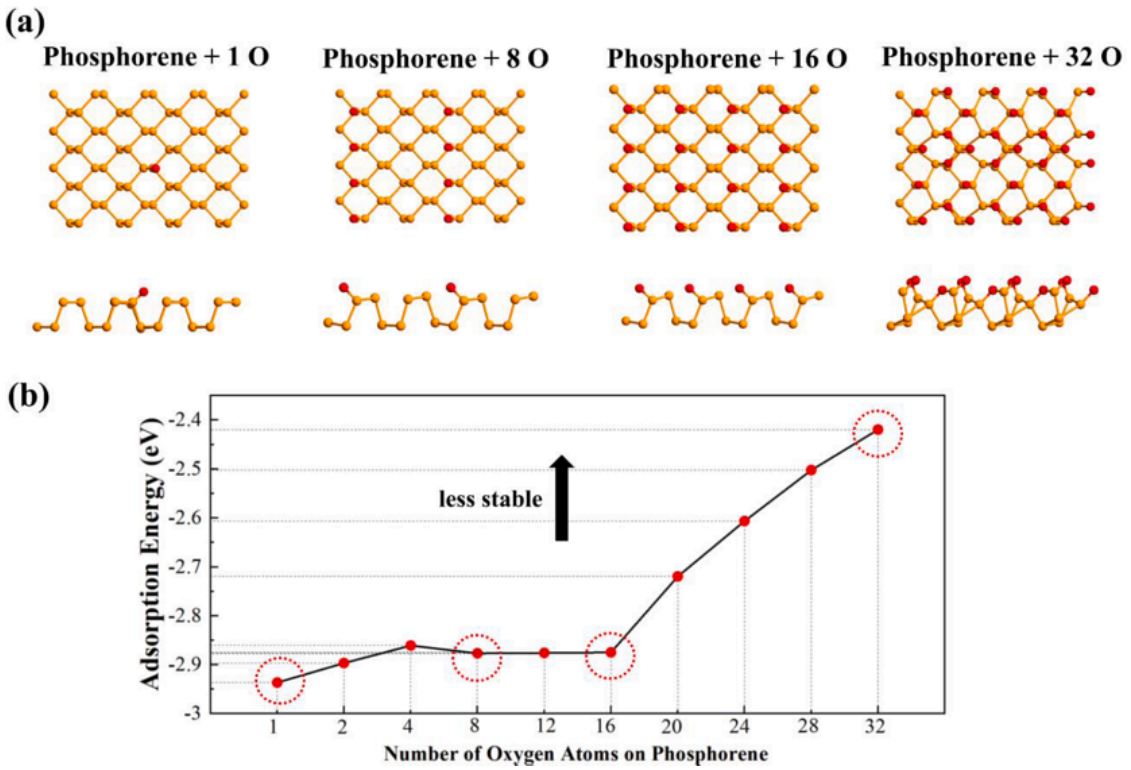

Fig. 3. (a) The representative structures of phosphorene oxides with 1, 8, 16, 32 oxygen atoms. (b) Adsorption energy per oxygen atom as a function of oxygen concentration calculated with the PBE functional (P: Orange and O: red).

Table 1
The calculated adsorption energy per oxygen atom (E_{ad}) and energy bandgap (E_g) for bare phosphorene and phosphorene oxide sheets with various oxygen concentrations.

System	$E_{ad\ per\ O\ atom}$ (eV)	E_g (eV)
Bare Phosphorene	-	0.92
Phosphorene + 1 O	2.93	0.98
Phosphorene + 2 O	2.89	1.03
Phosphorene + 4 O	2.86	1.06
Phosphorene + 8 O	2.87	1.09
Phosphorene + 12 O	2.87	0.90
Phosphorene + 16 O	2.87	0.85
Phosphorene + 20 O	2.71	0.98
Phosphorene + 24 O	2.60	1.12
Phosphorene + 28 O	2.50	0.91
Phosphorene + 32 O	2.41	0.37

atoms. It was reported that oxygen insertion into the phosphorene's lattice gives rise to considerable deformation, expanding the P-P distance and consequently increasing the local layer thickness [52]. This lattice deformation caused by oxygen insertion into the phosphorene promotes further oxidation in the neighborhood of the pre-existing oxygen defects. As a result, for a high enough oxygen concentration, the crystal could break apart due to this large stress [52]. From Fig. 3, the chemisorbed oxygen atoms always point away from the zigzag ridge. By adding more than 16 oxygen atoms to the structure, owing to the Coulomb interaction between their p orbitals, chemisorbed oxygen atoms repel each other, resulting in a reduction of the binding energy per O atom of the structure. It was reported that the electron density is mostly accumulated on the P–O bonds, while a moderate electron density distribution is seen on the oxygen. Therefore, for 32 oxygen atoms, we expect a much stronger Coulomb repulsion between dangling oxygens than bridging oxygens as also reported in Ref. [55].

The bandgap of phosphorene oxides depends on the oxygen concentration, suggesting that controlled oxidation can be used as a means to engineer the bandgap [55]. In a systematic study on the chemical functionalization of monolayer phosphorene by surface adsorption of fluorine and oxygen atoms, it is shown that in the case of fluorination most of the ground states are indirect bandgap semiconductors, and the majority of the oxide ground states are direct bandgap semiconductors [56,57]. Fig. S5 shows the energy band structures of phosphorene nanosheets with various oxygen concentrations. The bandgap slightly increases when a single oxygen atom is adsorbed. However, this defect is electrically neutral, as it introduces no states in the gap and the band structure is similar to that of pristine phosphorene. The bandgap values of the phosphorene oxides are comparable with that of pristine phosphorene, except for phosphorene with 32 oxygen atoms in which the bandgap drops to 0.37 eV. Although all oxide structures are direct bandgap semiconductors, phosphorene goes through a direct to indirect transition after oxidation with 32 oxygen atoms.

It should be mentioned that the oxygen affinity of the vacancy in phosphorene is much stronger than the perfect phosphorene lattice site. Upon exposure of an oxygen molecule to a vacancy in phosphorene, the O-O bond dissociates, and the resulting oxygen atoms react with P atoms. As a result, we expect that phosphorene fast degradation owing to oxidization is more likely to happen at edges and grain boundaries where vacancies tend to form [41].

In our DFT study, we only considered the adsorption and incorporation of oxygen atoms to find out if the O chemisorption is energetically favorable. Since the final aim is to exfoliate and deposit phosphorene on a solid support, we only discussed the scenario when phosphorene is oxygenated from one side. A more detalied study needs to be done to investigate the adsorption of oxygen at both sides of the phosphorene. The high adsorption energy obtained for an O atom on phosphorene suggests a chemisorption process and high sensitivity of phosphorene nanosheets to oxygen that is in good agreement with the TEM observations. Furthermore, our DFT data indicated that the breakage of P-P bonds in phosphorene upon oxidation results in amorphization, which correlates well with the TEM data observed in Fig. 2 (c-d). Future

research using in-situ TEM analysis could be done to better characterize the surface instability of the phosphorene nanosheets. It is believed that a better understanding of the defect and impurity of phosphorene nanosheet as well as the structure and property relationship, could be vital for the further application of the 2D materials.

4. Conclusion

In this study, we present a detailed study on defects in bipolar electrochemical exfoliated phosphorene nanosheets. Different types of point defects, area defects GBs as well as amorphous domains have been directly observed in phosphorene nanosheets via high-resolution TEM imaging. We observed that the exposure of phosphorene for several days to ambient conditions leads to very fast degradation of phosphorene nanosheets. Finally, DFT results disclosed that surface oxidation of the phosphorene caused the breakage of P-P bonds and the amorphization. The atomistic insight into the phosphorene nanosheets from our study will likely benefit future experimental and theoretical efforts on futuristic applications of phosphorene nanosheets.

CRediT authorship contribution statement

Amin Rabiei Baboukani: Conceptualization, Methodology, Formal analysis, Investigation, Writing – original draft, Writing – review & editing. **Sadegh Mehdi Aghaei:** Methodology, Investigation, Writing – original draft. **Iman Khakpour:** Formal analysis, Investigation. **Vadym Drozd:** Resources, Formal analysis, Investigation. **Aref Aasi:** Methodology. **Chunlei Wang:** Conceptualization, Writing – review & editing, Funding acquisition, Supervision.

Declaration of Competing Interest

The authors declare that they have no known competing financial interests or personal relationships that could have appeared to influence the work reported in this paper.

Acknowledgments

The authors would like to acknowledge Dr. Yusuf Emirov at University of South Florida for the experimental assistance and discussion. This work is partially supported by the US National Science Foundation awards 2107318 and 2126190, as well as Precise Advanced Technologies and Health Systems for Underserved Population (PATHS-UP) Engineering Research Center (ERC). A. Rabiei Baboukani acknowledges the Dissertation Year Fellowship (DYF) from Florida International University.

Supplementary materials

Supplementary material associated with this article can be found, in the online version, at doi:10.1016/j.susc.2022.122052.

References

[1] K.S. Novoselov, A.K. Geim, S.V. Morozov, D. Jiang, Y. Zhang, S.V. Dubonos, I. V. Grigorieva, A.A. Firsov, Electric field effect in atomically thin carbon films, Science 306 (2004) 666–669.
[2] Z. Zeng, Z. Yin, X. Huang, H. Li, Q. He, G. Lu, F. Boey, H. Zhang, Single-layer semiconducting nanosheets: high-yield preparation and device fabrication, Angew. Chem. 123 (2011) 11289–11293.
[3] W.-Q. Han, L. Wu, Y. Zhu, K. Watanabe, T. Taniguchi, Structure of chemically derived mono-and few-atomic-layer boron nitride sheets, Appl. Phys. Lett. 93 (2008), 223103.
[4] K. Kalantar-zadeh, J.Z. Ou, T. Daeneke, A. Mitchell, T. Sasaki, M.S. Fuhrer, Two dimensional and layered transition metal oxides, Appl. Mater. Today 5 (2016) 73–89.
[5] A. Rabiei Baboukani, I. Khakpour, V. Drozd, C. Wang, Liquid-based exfoliation of black phosphorus into phosphorene and its application for energy storage devices, Small Struct. (2021), 2000148.
[6] D.K. Sang, H. Wang, Z. Guo, N. Xie, H. Zhang, Recent developments in stability and passivation techniques of phosphorene toward next-generation device applications, Adv. Funct. Mater. 29 (2019), 1903419.
[7] Y. Tao, T. Huang, C. Ding, F. Yu, D. Tan, F. Wang, Q. Xie, S. Yao, Few-layer phosphorene: an emerging electrode material for electrochemical energy storage, Appl. Mater. Today 15 (2019) 18–33.
[8] T. Low, A. Rodin, A. Carvalho, Y. Jiang, H. Wang, F. Xia, A.C. Neto, Tunable optical properties of multilayer black phosphorus thin films, Phys. Rev. B 90 (2014), 075434.
[9] S. Witomska, T. Leydecker, A. Ciesielski, P. Samorì, Production and patterning of liquid phase–exfoliated 2D sheets for applications in optoelectronics, Adv. Funct. Mater. 29 (2019), 1901126.
[10] S. Yang, P. Zhang, A.S. Nia, X. Feng, Emerging 2D materials produced via electrochemistry, Adv. Mater. 32 (2020), 1907857.
[11] C. Xing, J. Zhang, J. Jing, J. Li, F. Shi, Preparations, properties and applications of low-dimensional black phosphorus, Chem. Eng. J. 370 (2019) 120–135.
[12] A.R. Baboukani, I. Khakpour, V. Drozd, A. Allagui, C. Wang, Single-step exfoliation of black phosphorus and deposition of phosphorene via bipolar electrochemistry for capacitive energy storage application, J. Mater. Chem. A 7 (2019) 25548–25556.
[13] A.R. Baboukani, I. Khakpour, C. Wang, Bipolar Exfoliation of Black Phosphorous into Phosphorene, Google Patents, 2020.
[14] Z. Lin, A. McCreary, N. Briggs, S. Subramanian, K. Zhang, Y. Sun, X. Li, N.J. Borys, H. Yuan, S.K. Fullerton-Shirey, 2D materials advances: from large scale synthesis and controlled heterostructures to improved characterization techniques, defects and applications, 2D Materials 3 (2016), 042001.
[15] Z. Wu, Z. Ni, Spectroscopic investigation of defects in two-dimensional materials, Nanophotonics 6 (2017) 1219–1237.
[16] Y. Guo, S. Zhou, J. Zhang, Y. Bai, J. Zhao, Atomic structures and electronic properties of phosphorene grain boundaries, 2D Materials 3 (2016), 025008.
[17] D. Rhodes, S.H. Chae, R. Ribeiro-Palau, J. Hone, Disorder in van der Waals heterostructures of 2D materials, Nat. Mater. 18 (2019) 541.
[18] J. Pei, X. Gai, J. Yang, X. Wang, Z. Yu, D.-Y. Choi, B. Luther-Davies, Y. Lu, Producing air-stable monolayers of phosphorene and their defect engineering, Nat. Commun. 7 (2016) 1–8.
[19] H.I. Rasool, C. Ophus, A. Zettl, Atomic defects in two dimensional materials, Adv. Mater. 27 (2015) 5771–5777.
[20] D. Muller, L.F. Kourkoutis, M. Murfitt, J. Song, H. Hwang, J. Silcox, N. Dellby, O. Krivanek, Atomic-scale chemical imaging of composition and bonding by aberration-corrected microscopy, Science 319 (2008) 1073–1076.
[21] P.Y. Huang, C.S. Ruiz-Vargas, A.M. Van Der Zande, W.S. Whitney, M.P. Levendorf, J.W. Kevek, S. Garg, J.S. Alden, C.J. Hustedt, Y. Zhu, Grains and grain boundaries in single-layer graphene atomic patchwork quilts, Nature 469 (2011) 389–392.
[22] J. Hong, C. Jin, J. Yuan, Z. Zhang, Atomic defects in two-dimensional materials: from single-atom spectroscopy to functionalities in opto-/electronics, nanomagnetism, and catalysis, Adv. Mater. 29 (2017), 1606434.
[23] T. Susi, D. Kepaptsoglou, Y.-C. Lin, Q.M. Ramasse, J.C. Meyer, K. Suenaga, J. Kotakoski, Towards atomically precise manipulation of 2D nanostructures in the electron microscope, 2D Materials 4 (2017), 042004.
[24] A.E. Naclerio, D.N. Zakharov, J. Kumar, B. Rogers, C.L. Pint, M. Shrivastava, P. R. Kidambi, Visualizing oxidation mechanisms in few-layered black phosphorus via in situ transmission electron microscopy, ACS Appl. Mater. Interfaces 12 (2020) 15844–15854.
[25] C. Hyun, J.H. Kim, J.-Y. Lee, G.-H. Lee, K.S. Kim, Atomic scale study of black phosphorus degradation, RSC Adv. 10 (2020) 350–355.
[26] M. van Druenen, F.n. Davitt, T. Collins, C. Glynn, C. O'Dwyer, J.D. Holmes, G. Collins, Evaluating the surface chemistry of black phosphorus during ambient degradation, Langmuir 35 (2019) 2172–2178.
[27] K.L. Kuntz, R.A. Wells, J. Hu, T. Yang, B. Dong, H. Guo, A.H. Woomer, D.L. Druffel, A. Alabanza, D. Tománek, Control of surface and edge oxidation on phosphorene, ACS Appl. Mater. Interfaces 9 (2017) 9126–9135.
[28] Y. Cai, Q. Ke, G. Zhang, B.I. Yakobson, Y.-W. Zhang, Highly itinerant atomic vacancies in phosphorene, J. Am. Chem. Soc. 138 (2016) 10199–10206.
[29] V. Wang, Y. Kawazoe, W. Geng, Native point defects in few-layer phosphorene, Phys. Rev. B 91 (2015), 045433.
[30] W. Hu, J. Yang, Defects in phosphorene, J. Phys. Chem. C 119 (2015) 20474–20480.
[31] X. Li, L. Ma, D. Wang, X.C. Zeng, X. Wu, J. Yang, Point defects in lines in single crystalline phosphorene: directional migration and tunable band gaps, Nanoscale 8 (2016) 17801–17808.
[32] Y. Liu, F. Xu, Z. Zhang, E.S. Penev, B.I. Yakobson, Two-dimensional mono-elemental semiconductor with electronically inactive defects: the case of phosphorus, Nano Lett. 14 (2014) 6782–6786.
[33] J. Taylor, H. Guo, J. Wang, Ab initio modeling of quantum transport properties of molecular electronic devices, Phys. Rev. B 63 (2001), 245407.
[34] M. Brandbyge, J.-L. Mozos, P. Ordejón, J. Taylor, K. Stokbro, Density-functional method for nonequilibrium electron transport, Phys. Rev. B 65 (2002), 165401.
[35] Q. Simulator, Atomistix ToolKit (ATK), 2012.
[36] S. Grimme, Semiempirical GGA-type density functional constructed with a long-range dispersion correction, J. Comput. Chem. 27 (2006) 1787–1799.
[37] S. Grimme, C. Mück-Lichtenfeld, J. Antony, Noncovalent interactions between graphene sheets and in multishell (hyper) fullerenes, J. Phys. Chem. C 111 (2007) 11199–11207.
[38] D.C. Liu, J. Nocedal, On the limited memory BFGS method for large scale optimization, Math. Program. 45 (1989) 503–528.

[39] H.J. Monkhorst, J.D. Pack, Special points for Brillouin-zone integrations, Phys. Rev. B 13 (1976) 5188.
[40] S.F. Boys, F. Bernardi, The calculation of small molecular interactions by the differences of separate total energies. Some procedures with reduced errors, Mol. Phys. 19 (1970) 553–566.
[41] A.A. Kistanov, Y. Cai, K. Zhou, S.V. Dmitriev, Y.-W. Zhang, The role of H2O and O2 molecules and phosphorus vacancies in the structure instability of phosphorene, 2D Materials 4 (2016), 015010.
[42] U. Bangert, A. Stewart, E. O'Connell, E. Courtney, Q. Ramasse, D. Kepaptsoglou, H. Hofsäss, J. Amani, J.-S. Tu, B. Kardynal, Ion-beam modification of 2-D materials-single implant atom analysis via annular dark-field electron microscopy, Ultramicroscopy 176 (2017) 31–36.
[43] Z.-L. Zhu, W.-Y. Yu, X.-Y. Ren, Q. Sun, Y. Jia, Grain boundary in phosphorene and its unique roles on C and O doping, EPL (Europhys. Lett.) 109 (2015) 47003.
[44] A. Castellanos-Gomez, L. Vicarelli, E. Prada, J.O. Island, K. Narasimha-Acharya, S. I. Blanter, D.J. Groenendijk, M. Buscema, G.A. Steele, J. Alvarez, Isolation and characterization of few-layer black phosphorus, 2D Materials 1 (2014), 025001.
[45] D. Grasseschi, D. Bahamon, F. Maia, A.C. Neto, R. Freitas, C. De Matos, Oxygen impact on the electronic and vibrational properties of black phosphorus probed by synchrotron infrared nanospectroscopy, 2D Materials 4 (2017), 035028.
[46] Y. Huang, J. Qiao, K. He, S. Bliznakov, E. Sutter, X. Chen, D. Luo, F. Meng, D. Su, J. Decker, W. Ji, R.S. Ruoff, P. Sutter, Interaction of black phosphorus with oxygen and water, Chem. Mater. 28 (2016) 8330–8339.
[47] W. Luo, D.Y. Zemlyanov, C.A. Milligan, Y. Du, L. Yang, Y. Wu, D.Y. Peide, Surface chemistry of black phosphorus under a controlled oxidative environment, Nanotechnology 27 (2016), 434002.
[48] V. Vierimaa, A.V. Krasheninnikov, H.-P. Komsa, Phosphorene under electron beam: from monolayer to one-dimensional chains, Nanoscale 8 (2016) 7949–7957.
[49] H. Liu, A.T. Neal, Z. Zhu, Z. Luo, X. Xu, D. Tománek, P.D. Ye, Phosphorene: an unexplored 2D semiconductor with a high hole mobility, ACS Nano 8 (2014) 4033–4041.
[50] S.Y. Lei, Z.Y. Yu, H.Y. Shen, X.L. Sun, N. Wan, H. Yu, CO adsorption on metal-decorated phosphorene, ACS Omega 3 (2018) 3957–3965.
[51] A. Ferretti, G. Mallia, L. Martin-Samos, G. Bussi, A. Ruini, B. Montanari, N. M. Harrison, Ab initio complex band structure of conjugated polymers: Effects of hydrid density functional theory and GW schemes, Phys. Rev. B 85 (2012), 235105.
[52] A. Ziletti, A. Carvalho, D.K. Campbell, D.F. Coker, A.C. Neto, Oxygen defects in phosphorene, Phys. Rev. Lett. 114 (2015), 046801.
[53] S. Aghaei, M. Monshi, I. Calizo, A theoretical study of gas adsorption on silicene nanoribbons and its application in a highly sensitive molecule sensor, RSC Adv. 6 (2016) 94417–94428.
[54] G. Wang, W.J. Slough, R. Pandey, S.P. Karna, Degradation of phosphorene in air: understanding at atomic level, 2D Materials 3 (2016), 025011.
[55] A. Ziletti, A. Carvalho, P. Trevisanutto, D. Campbell, D. Coker, A.C. Neto, Phosphorene oxides: bandgap engineering of phosphorene by oxidation, Phys. Rev. B 91 (2015), 085407.
[56] S. Nahas, B. Ghosh, S. Bhowmick, A. Agarwal, First-principles cluster expansion study of functionalization of black phosphorene via fluorination and oxidation, Phys. Rev. B 93 (2016), 165413.
[57] Z. Wang, D. Zhao, S. Yu, Z. Nie, Y. Li, L. Zhang, First-principles investigation of structural and electronic properties of oxygen adsorbing phosphorene, Progr. Natural Sci. 29 (2019) 316–321.